
Twin Auxiliary Classifiers GAN

Mingming Gong^{*§} Yanwu Xu^{*†} Chunyuan Li[‡] Kun Zhang[§] Kayhan Batmanghelich[†]

Abstract

Conditional generative models enjoy remarkable progress over the past few years. One of the popular conditional models is Auxiliary Classifier GAN (AC-GAN), which generates highly discriminative images by extending the loss function of GAN with an auxiliary classifier. However, the diversity of the generated samples by AC-GAN tends to decrease as the number of classes increases, hence limiting its power on large-scale data. In this paper, we identify the source of the low diversity issue theoretically and propose a practical solution to solve the problem. We show that the auxiliary classifier in AC-GAN imposes perfect separability, which is disadvantageous when the supports of the class distributions have significant overlap. To address the issue, we propose Twin Auxiliary Classifiers Generative Adversarial Net (TAC-GAN) that further benefits from a new player that interacts with other players (the generator and the discriminator) in GAN. Theoretically, we demonstrate that TAC-GAN can effectively minimize the divergence between the generated and real-data distributions. Extensive experimental results show that our TAC-GAN can successfully replicate the true data distributions on simulated data, and significantly improves the diversity of class-conditional image generation on real datasets.

1 Introduction

Generative Adversarial Networks (GANs) [1] are a framework to learn the data generating distribution implicitly. GANs mimic sampling from a target distribution by training a generator that maps samples drawn from a canonical distribution to the data space. A distinctive feature of GANs is that the discriminator that evaluates the separability of the real and generated data distributions [1–4]. If the discriminator can hardly distinguish between real and generated data, the generator is likely to provide a good approximation to the true data distribution. To generate high-fidelity images, much recent research has focused on designing more advanced network architectures [5, 6], developing more stable objective functions [7–9, 3], enforcing appropriate constraints on the discriminator [10–12], or improving training techniques [7, 13].

Conditional GANs (cGANs) [14] are a variant of GANs that take advantage of extra information (condition) and have been widely used for generation of class-conditioned images [15–18] and text [19, 20]. A major difference between cGANs and GANs is that the cGANs feed the condition to both the generator and the discriminator to learn the joint distributions of images and the condition random variables. Most methods feed the conditional information by concatenating it (or its embedding) with the input or the feature vector at specific layers [14, 21, 15, 22, 23, 20]. Recently, Projection-cGAN [24] improves the quality of the generated images using a specific discriminator that takes the inner product between the embedding of the conditioning variable and the feature vector of the input image, obtaining state-of-the-art class-conditional image generation on large-scale datasets such as ImageNet1000 [25].

^{*}Equal Contribution

[†]University of Pittsburgh, USA

[‡]Microsoft Research, Redmond, USA

[§]Carnegie Mellon University, USA

Among cGANs, the Auxiliary Classifier GAN (AC-GAN) has received much attention due to its simplicity and extensibility to various applications [17]. AC-GAN incorporates the conditional information (label) by training the GAN discriminator with an additional classification loss. AC-GAN is able to generate high-quality images and has been extended to various learning problems, such as text-to-image generation [26]. However, it is reported in the literature [17, 24] that as the number of labels increases, AC-GAN tends to generate near-identical images for most classes. Miyato *et al.* [24] observed this phenomenon on ImageNet1000 and conjectured that the auxiliary classifier might encourage the generator to produce less diverse images so that they can be easily discernable.

Despite these insightful findings, the exact source of the low-diversity problem is unclear, let alone its remedy. In this paper, we aim to provide an understanding of this phenomenon and accordingly develop a new method that is able to generate diverse and realistic images. First, we show that due to a missing term in the objective of AC-GAN, it does not faithfully minimize the divergence between real and generated conditional distribution. We show that missing that term can result in a degenerate solution, which explains the lack of diversity in the generated data. Based on our understanding, we introduce a new player in the min-max game of AC-GAN that enables us to estimate the missing term in the objective. The resulting method properly estimates the divergence between real and generated conditional distributions and significantly increases sample diversity within each class. We call our method Twin Auxiliary Classifiers GAN (TAC-GAN) since the new player is also a classifier. Compared to AC-GAN, our TAC-GAN successfully replicates the real data distributions on simulated data and significantly improves the quality and diversity of the class-conditional image generation on CIFAR100 [27], VGGFace2 [28], and ImageNet1000 [25] datasets. In particular, to our best knowledge, our TAC-GAN is the first cGAN method that can generate good quality images on the VGGFace dataset, demonstrating the advantage of TAC-GAN on fine-grained datasets.

2 Method

In this section, we review the Generative Adversarial Network (GAN) [1] and its conditional variant (cGAN) [14]. We review one of the most popular variants of cGAN, which is called Auxiliary Classifier GAN (AC-GAN) [17]. We first provide an understanding of the observation of low-diversity samples generated by AC-GAN from a distribution matching perspective. Second, based on our new understanding of the problem, we propose a new method that enables learning of real distributions and increasing sample diversity.

2.1 Background

Given a training set $\{\mathbf{x}_i\}_{i=1}^n \subseteq \mathcal{X}$ drawn from an unknown distribution P_X , GAN estimates P_X by specifying a distribution Q_X implicitly. Instead of an explicit parametrization, it trains a generator function $G(Z)$ that maps samples from a canonical distribution, i.e., $Z \sim P_Z$, to the training data. The generator is obtained by finding an equilibrium of the following mini-max game that effectively minimizes the Jensen-Shannon Divergence (JSD) between Q_X and P_X :

$$\min_G \max_D \mathbb{E}_{X \sim P_X} [\log D(X)] + \mathbb{E}_{Z \sim P_Z} [\log(1 - D(G(Z)))] \quad (1)$$

where D is a discriminator. Notice that the Q_X is not directly modeled.

Given a pair of observation (\mathbf{x}) and a condition (y), $\{\mathbf{x}_i, y\}_{i=1}^n \subseteq \mathcal{X} \times \mathcal{Y}$ drawn from the joint distribution $(\mathbf{x}_i, y) \sim P_{XY}$, the goal of cGAN is to estimate a conditional distribution $P_{X|Y}$. Let $Q_{X|Y}$ denote the conditional distribution specified by a generator $G(Y, Z)$ and $Q_{XY} := Q_{X|Y}P_Y$. A generic cGAN trains G to implicitly minimize the JSD divergence between the joint distributions Q_{XY} and P_{XY} :

$$\min_G \max_D \mathbb{E}_{(X, Y) \sim P_{XY}} [\log D(X, Y)] + \mathbb{E}_{Z \sim P_Z, Y \sim P_Y} [\log(1 - D(G(Z, Y), Y))] \quad (2)$$

In general, Y can be a continuous or discrete variable. In this paper, we focus on case that Y is the (discrete) class label, *i.e.*, $\mathcal{Y} = \{1, \dots, K\}$.

2.2 Insight on Auxiliary Classifier GAN (AC-GAN)

AC-GAN introduces a new player C which is a classifier that interacts with the D and G players. We use $Q_{Y|X}^c$ to denote the conditional distribution induced by C . The AC-GAN optimization combines

the original GAN loss with cross-entropy classification loss:

$$\min_{G,C} \max_D \mathcal{L}_{\text{AC}}(G, D, C) = \underbrace{\mathbb{E}_{X \sim P_X} [\log D(X)] + \mathbb{E}_{Z \sim P_Z, Y \sim P_Y} [\log(1 - D(G(Z, Y)))]}_{\textcircled{a}} - \lambda_c \underbrace{\mathbb{E}_{(X,Y) \sim P_{XY}} [\log C(X, Y)]}_{\textcircled{b}} - \lambda_c \underbrace{\mathbb{E}_{Z \sim P_Z, Y \sim P_Y} [\log(C(G(Z, Y), Y))]}_{\textcircled{c}}, \quad (3)$$

where λ_c is a hyperparameter balancing GAN and auxiliary classification losses.

Here we decompose the objective of AC-GAN into three terms. Clearly, the first term \textcircled{a} corresponds to the Jensen-Shannon divergence (JSD) between Q_X and P_X . The second term \textcircled{b} is the cross-entropy loss on real data. It is straightforward to show that the second term minimizes Kullback-Leibler (KL) divergence between the real data distribution $P_{Y|X}$ and the distribution $Q_{Y|X}^c$ specified by C . To show that, we can add the negative conditional entropy, $-H_P(Y|X) = \mathbb{E}_{(X,Y) \sim P_{XY}} [\log P(Y|X)]$, to \textcircled{b} , we have

$$\begin{aligned} -H_P(Y|X) + \textcircled{b} &= \mathbb{E}_{(X,Y) \sim P_{XY}} [\log P(Y|X)] - \mathbb{E}_{(X,Y) \sim P_{XY}} [\log C(X, Y)] \\ &= \mathbb{E}_{(X,Y) \sim P_{XY}} [\log P(Y|X)] - \mathbb{E}_{(X,Y) \sim P_{XY}} [\log Q^c(Y|X)] \\ &= \mathbb{E}_{(X,Y) \sim P_{XY}} \left[\log \frac{P(Y|X)}{Q^c(Y|X)} \right] = \text{KL}(P_{Y|X} || Q_{Y|X}^c). \end{aligned} \quad (4)$$

Since the negative conditional entropy $-H_P(Y|X)$ is a constant term, minimizing \textcircled{b} w.r.t. the network parameters in C effectively minimizes the KL divergence between $P_{Y|X}$ and $Q_{Y|X}^c$.

The third term \textcircled{c} is the cross-entropy loss on the generated data. Similarly, if one adds the negative entropy $-H_Q(Y|X) = \mathbb{E}_{(X,Y) \sim Q_{XY}} [\log Q(Y|X)]$ to \textcircled{c} and obtain the following result:

$$-H_Q(Y|X) + \textcircled{c} = \mathbb{E}_{(X,Y) \sim Q_{XY}} [\log Q(Y|X)] - \mathbb{E}_{(X,Y) \sim Q_{XY}} [\log Q^c(Y|X)] = \text{KL}(Q_{Y|X} || Q_{Y|X}^c).$$

When updating C , $-H_Q(Y|X)$ can be considered a constant term, thus minimizing \textcircled{c} w.r.t. C effectively minimizes the KL divergence between $Q_{Y|X}$ and $Q_{Y|X}^c$. However, when updating G , $-H_Q(Y|X)$ cannot be considered as a constant term, because $Q_{Y|X}$ is the conditional distribution specified by the generator G . AC-GAN ignores $-H_Q(Y|X)$ and only minimizes \textcircled{c} when updating G in the optimization procedure, which fails to minimize the KL divergence between $Q_{Y|X}$ and $Q_{Y|X}^c$. We hypothesize that the likely reason behind low diversity samples generated by AC-GAN is that it fails to account for the missing term while updating G . In fact, the following theorem shows that AC-GAN can converge to a degenerate distribution:

Theorem 1. Suppose $P_X = Q_X$. Given an auxiliary classifier C which specifies a conditional distribution $Q_{Y|X}^c$, the optimal G^* that minimizes \textcircled{c} induces the following degenerate conditional distribution $Q_{Y|X}^*$,

$$Q^*(Y = k|X = x) = \begin{cases} 1, & \text{if } k = \arg \max_i Q^c(Y = i|X = x), \\ 0, & \text{otherwise.} \end{cases} \quad (5)$$

Proof is given in Section S1 of the Supplementary Material (SM). Theorem 1 shows that, even when the marginal distributions are perfectly matched by GAN loss \textcircled{a} , AC-GAN is not able to model the probability when class distributions have support overlaps. It tends to generate data in which Y is deterministically related to X . This means that the generated images for each class are confined by the regions induced by the decision boundaries of the auxiliary classifier C , which fails to replicate conditional distribution $Q_{Y|X}^c$, implied by C , and reduces the distributional support of each class. The theoretical result is consistent with the empirical results in [24] that AC-GAN generates discriminable images with low intra-class diversity. It is thus essential to incorporate the missing term, $-H_Q(Y|X)$, in the objective to penalize this behavior and minimize the KL divergence between $Q_{Y|X}$ and $Q_{Y|X}^c$.

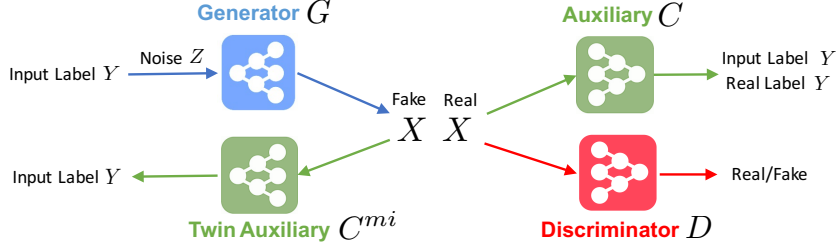


Figure 1: Illustration of the proposed TAC-GAN. The generator G synthesizes fake samples X conditioned input label Y . The discriminator D distinguishes between real/fake samples. The auxiliary classifier C is trained to classify labels on both real and fake pairs, while the proposed twin auxiliary classifier C^{mi} is trained on fake pairs only.

2.3 Twin Auxiliary Classifiers GAN (TAC-GAN)

Our analysis in the previous section motivates adding the missing term, $-H_Q(Y|X)$, back to the objective function. While minimizing \textcircled{C} forces G to concentrate the conditional density mass on the training data, $-H_Q(Y|X)$ works in the opposite direction by increasing the entropy. However, estimating $-H_Q(Y|X)$ is a challenging task since we do not have access to $Q_{Y|X}$. Various methods have been proposed to estimate the (conditional) entropy, such as [29–32]; however, these estimators cannot be easily used as an objective function to learn G via backpropagation. Below we propose to estimate the conditional entropy by adding a new player in the mini-max game.

The general idea is to introduce an additional auxiliary classifier, C^{mi} , that aims to identify the labels of the samples drawn from $Q_{X|Y}$; the low-diversity case makes this task easy for C^{mi} . Similar to GAN, the generator tries to compete with the C^{mi} . The overall idea of TAC-GAN is illustrated in Figure 1. In the following, we demonstrate its connection with minimizing $-H_Q(Y|X)$.

Proposition: Let us assume, without loss of generality, that all classes are equally likely⁵ (i.e., $P(Y = k) = \frac{1}{K}$). Minimizing $-H_Q(Y|X)$ is equivalent to minimizing (1) the mutual information between Y and X and (2) the JSD between the conditional distributions $\{Q_{X|Y=1}, \dots, Q_{X|Y=K}\}$.

Proof.

$$\begin{aligned}
 I_Q(Y, X) &= H(Y) - H_Q(Y|X) = H_Q(X) - H_Q(X|Y) \\
 &= -\frac{1}{K} \sum_{k=1}^K \mathbb{E}_{X \sim Q_{X|Y=k}} \log Q(X) + \frac{1}{K} \sum_{k=1}^K \mathbb{E}_{X \sim Q_{X|Y=k}} \log Q(X|Y = k) \\
 &= \frac{1}{K} \sum_{k=1}^K \text{KL}(Q_{X|Y=k} || Q_X) = \text{JSD}(Q_{X|Y=1}, \dots, Q_{X|Y=K}).
 \end{aligned} \tag{6}$$

(1) follows from the fact that entropy of Y is constant with respect to Q , (2) is shown above. \square

Based on the connection between $-H_Q(Y|X)$ and JSD, we extend the two-player minimax approach in GAN [1] to minimize the JSD between multiple distributions. More specifically, we use another auxiliary classifier C^{mi} whose last layer is a softmax function that predicts the probability of X belong to a class $Y = k$. We define the following minimax game:

$$\min_G \max_{C^{mi}} V(G, C^{mi}) = \mathbb{E}_{Z \sim P_Z, Y \sim P_Y} [\log(C^{mi}(G(Z, Y), Y))]. \tag{7}$$

The following theorem shows that the minimax game can effectively minimize the JSD between $\{Q_{X|Y=1}, \dots, Q_{X|Y=K}\}$.

Theorem 2. Let $U(G) = \max_{C^{mi}} V(G, C^{mi})$. The global minimum of the minimax game is achieved if and only if $Q_{X|Y=1} = Q_{X|Y=2} = \dots = Q_{X|Y=K}$. At the optimal point, $U(G)$ achieves the value $-K \log K$.

⁵If the dataset is imbalanced, we can apply biased batch sampling to enforce this condition.

A complete proof of Theorem 2 is given in Section S2 of the SM. It is worth noting that the global optimum of $U(G)$ cannot be achieved in our model because of other terms in our TAC-GAN objective function, which is obtained by combining (E3) and the original AC-GAN objective (3):

$$\min_{G,C} \max_{D,C^{mi}} \mathcal{L}_{\text{TAC}}(G, D, C, C^{mi}) = \mathcal{L}_{\text{AC}}(G, D, C) + \lambda_c V(G, C^{mi}). \quad (8)$$

The following theorem provides approximation guarantees for the joint distribution P_{XY} , justifying the validity of our proposed approach.

Theorem 3. *Let $P_{Y|X}$ and $Q_{Y|X}$ denote the data distribution and the distribution specified by the generator G , respectively. Let $Q_{Y|X}^c$ denote the conditional distribution of Y given X specified by the auxiliary classifier C . We have*

$$JSD(P_{XY}, Q_{XY}) \leq 2c_1 \sqrt{2JSD(P_X, Q_X)} + c_2 \sqrt{2KL(P_{Y|X} || Q_{Y|X}^c)} + c_2 \sqrt{2KL(Q_{Y|X} || Q_{Y|X}^c)},$$

where c_1 and c_2 are upper bounds of $\frac{1}{2} \int |P_{Y|X}(y|x)|\mu(x, y)$ and $\frac{1}{2} \int |Q_X(x)|\mu(x)$ (μ is a σ -finite measure), respectively. A proof of Theorem 3 is provided in Section S3 of the SM.

3 Related Works

TAC-GAN learns an unbiased distribution. Shu *et al.* [33] first show that AC-GAN tends to down-sample the data points near the decision boundary, causing a biased estimation of the true distribution. From a Lagrangian perspective, they consider AC-GAN as minimizing $JSD(P_X, Q_X)$ with constraints enforced by classification losses. If λ_c is very large such that $JSD(P_X, Q_X)$ become less effective, the generator will push the generated images away from the boundary. However, on real datasets, we can also observe low diversity when λ_c is small, which cannot be explained by the analysis in [33]. We take a different perspective by constraining $JSD(P_X, Q_X)$ to be small and investigate the properties of the conditional $Q_{Y|X}$. Our analysis suggests that even when $JSD(P_X, Q_X) = 0$, the AC-GAN cross-entropy loss can still result in biased estimate of $Q_{Y|X}$, reducing the support of each class in the generated distribution, compared to the true distribution. Furthermore, we propose a solution that can remedy the low diversity problem based on our understandings.

Connecting TAC-GAN with Projection cGAN. AC-GAN was once the state-of-the-art method before the advent of Projection cGAN [24]. Projection cGAN, AC-GAN, and our TAC-GAN share the similar spirits in that image generation performance can be improved when the joint distribution matching problem is decomposed into two easier sub-problems: marginal matching and conditional matching [32]. Projection cGAN decomposes the density ratio, while AC-GAN and TAC-GAN directly decompose the distribution. Both Projection cGAN and TAC-GAN are theoretically sound when using the cross-entropy loss. However, in practice, hinge loss is often preferred for real data. In this case, Projection cGAN loses the theoretical guarantee, while TAC-GAN is less affected, because only the GAN loss is replaced by the hinge loss.

4 Experiments

We first compare the distribution matching ability of AC-GAN, Projection cGAN, and our TAC-GAN on Mixture of Gaussian (MoG) and MNIST [34] synthetic data. We evaluate the image generation performance of TAC-GAN on three image datasets including CIFAR100 [27], ImageNet1000 [25] and VGGFace2 [28]. In our implementation, the twin auxiliary classifiers share the same convolutional layers, which means TAC-GAN only adds a negligible computation cost to AC-GAN. The detailed experiment setups are shown in the SM. We implemented TAC-GAN in Pytorch. To illustrate the algorithm, we submit the implementation on the synthetic datasets in SM. The source code to reproduce the full experimental results will be made public on GitHub.

4.1 MoG Synthetic Data

We start with a simulated dataset to verify that TAC-GAN can accurately match the target distribution. We draw samples from a one-dimensional MoG distribution with three Gaussian components, labeled

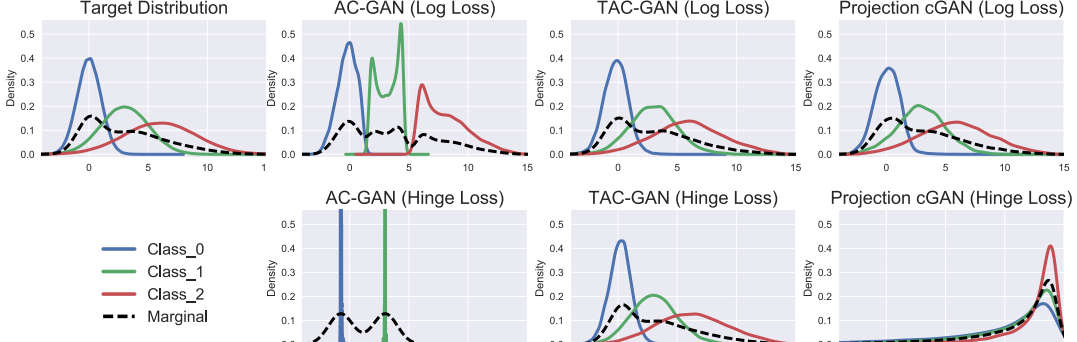


Figure 2: Comparison of sample quality on a synthetic MoG dataset.

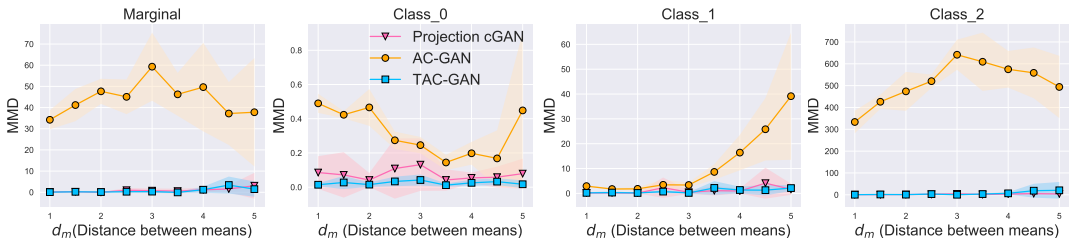


Figure 3: The MMD evaluation. The x-axis means the distance between the means of adjacent Gaussian components (d_m). Lower score is better.

as Class_0, Class_1, and Class_2, respectively. The standard deviations of the three components are fixed to $\sigma_0 = 1$, $\sigma_1 = 2$, and $\sigma_2 = 3$. The differences between the means are set to $\mu_1 - \mu_0 = \mu_2 - \mu_1 = d_m$, in which d_m ranges from 1 to 5. These values are chosen such that the supports of the three distributions have different overlap sizes. We detail the experimental setup in Section S4 of the SM.

Figure 2 shows the ground truth density functions when $\mu_0 = 0$, $\mu_1 = 3$, $\mu_2 = 6$ and the estimated ones by AC-GAN, TAC-GAN, and Projection cGAN. The estimated density function is obtained by applying kernel density estimation [35] on the generated data. When using cross-entropy loss, AC-GAN learns a biased distribution where all the classes are perfectly separated by the classification decision function, verifying our Theorem 1. Both our TAC-GAN and Projection cGAN can accurately learn the original distribution. Using Hinge loss, our model can still learn the distribution well, while neither AC-GAN nor Projection cGAN can replicate the real distribution (see Supplementary S4 for more experiments). We also conduct simulation on a 2D dataset and the details are given in Supplementary S5. The results show that our TAC-GAN is able to learn the true data distribution.

Figure 3 reports the Maximum Mean Discrepancy (MMD) [36] distance between the real data and generated data for different d_m values. Here all the GAN models are trained using cross-entropy loss (log loss). The TAC-GAN produces near-zero MMD values for all d_m 's, meaning that the data generated by TAC-GAN is very close to the ground truth data. Projection cGAN performs slightly worse than TAC-GAN and AC-GAN generates data that have a large MMD distance to the true data.

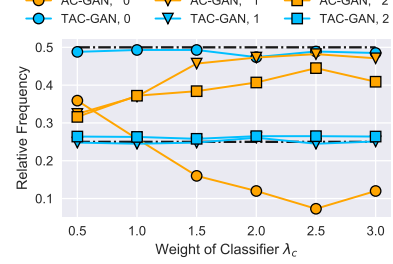
4.2 Overlapping MNIST

Following experiments in [33] to show that AC-GAN learns a biased distribution, we use the overlapping MNIST dataset to demonstrate the robustness of our TAC-GAN. We randomly sample from MNIST training set to construct two image groups: Group A contains 5,000 digit ‘1’ and 5,000 digit ‘0’, while Group B contains 5,000 digit ‘2’ and 5,000 digit ‘0’, to simulate overlapping distributions, where digit ‘0’ appears in both groups. Note that the ground truth proportion of digit ‘0’, ‘1’ and ‘2’ in this dataset are 0.5, 0.25 and 0.25, respectively.

Figure 4 (a) shows the generated images under different λ_c . It shows that AC-GAN tends to down sample ‘0’ as λ_c increases, while TAC-GAN can always generate ‘0’s in both groups. To quantitatively measure the distribution of generated images, we pre-train a “perfect” classifier on a MNIST subset

Real Data	
AC-GAN, $\lambda_c = 1$	
TAC-GAN, $\lambda_c = 1$	
AC-GAN, $\lambda_c = 2$	
TAC-GAN, $\lambda_c = 2$	

(a) Generated samples



(b) Quantitative result

Figure 4: (a) Visualization of the generated MNIST digits with various λ_c values. For each section, the top row digits are sampled from group A and the bottom row digits are from group B . (b) The label proportion for generated digits of two methods. The ground truth proportion for digit 0,1,2 is [0.5, 0.25, 0.25], visualized as dashed dark lines.

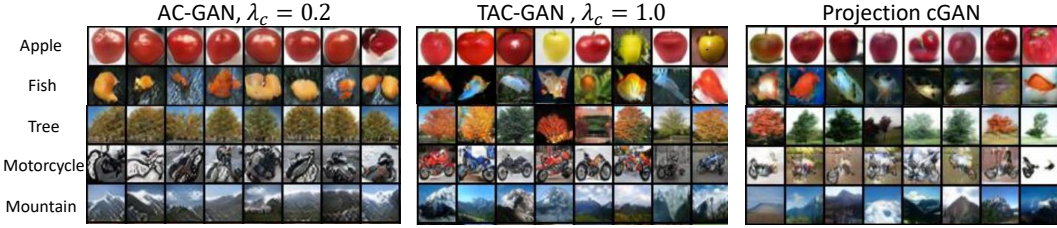


Figure 5: Generated images from five classes of CIFAR100.

only containing digit ‘0’, ‘1’, and ‘2’, and use the classifier to predict the labels of the generated data. Figure 4 (b) reports the label proportions for the generated images. It shows that the label proportion produced by TAC-GAN is very close to the ground truth values regardless of λ_c , while AC-GAN generates less ‘0’s as λ_c increases. More results and detail setting are shown in Section S6 of the SM.

4.3 CIFAR100

CIFAR100 [27] has 100 classes, each of which contains 500 training images and 100 testing images at the resolution of 32×32 . The current best deep classification model achieves 91.3% accuracy on this dataset [37], which suggests that the class distributions may have certain support overlaps.

Figure 5 shows the generated images for five randomly selected classes. AC-GAN generates images with low intra-class diversity. Both TAC-GAN and Projection cGAN generate visually appealing and diverse images. We provide the generated images for all the classes in Section S6 of the SM.

To quantitatively compare the generated images, we consider the two popular evaluation criteria, including Inception Score (IS) [38] and Fréchet Inception Distance (FID) [39]. We also use the recently proposed Learned Perceptual Image Patch Similarity (LPIPS), which measures the perceptual diversity within each class [40]. The scores are reported in Table 1. TAC-GAN achieves lower FID than Projection cGAN, and outperforms AC-GAN by a large margin, which demonstrates the efficacy of the twin auxiliary classifiers. We report the scores for all the classes in Section S7 of the SM.

Effects of hyper-parameters λ_c . We study the impact of λ_c on AC-GAN and TAC-GAN, and report results under different λ_c values in Figure 6. It shows that TAC-GAN is robust to λ_c , while AC-GAN requires a very small λ_c to achieve good scores. Even so, AC-GAN generates images with low intra-class diversity, as shown in Figure 5.

4.4 ImageNet1000

We further apply TAC-GAN to the large-scale ImageNet dataset [25] containing 1000 classes, each of which has around 1,300 images. We pre-process the data by center-cropping and resizing the images to 128×128 . We detail the experimental setup and attach generated images in Section S8 of the SM.

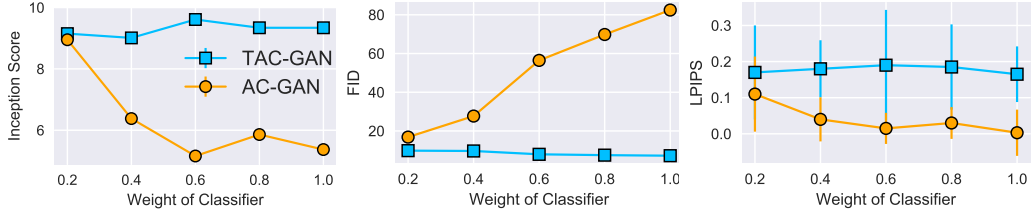


Figure 6: Impact of λ_c on the image generation quality on CIFAR100.



Figure 7: Comparison of generated face samples from three identities in VGGFace2 dataset.

Table 1: The quantitative results of all models on three datasets.

Metrics	AC-GAN ($\lambda_c = 1$)			TAC-GAN (Ours) ($\lambda_c = 1$)			Projection cGAN		
	IS \uparrow	FID \downarrow	LPIPS \uparrow	IS \uparrow	FID \downarrow	LPIPS \uparrow	IS \uparrow	FID \downarrow	LPIPS \uparrow
CIFAR100	5.37 \pm 0.064	82.45	0.003	9.34 \pm 0.077	7.22	0.165	9.56 \pm 0.133	8.92	0.169
ImageNet1000	7.26 \pm 0.113	184.41	0.058	28.86 \pm 0.298	23.75	0.634	38.05 \pm 0.790	22.77	0.616
VGGFace200	27.81 \pm 0.29	95.70	0.023	48.94 \pm 0.63	29.12	0.260	32.50 \pm 0.44	66.23	0.270
VGGFace500	25.96 \pm 0.32	31.90	0.031	77.76 \pm 1.61	12.42	0.269	35.96 \pm 0.62	43.10	0.130

Table 1 reports the IS, FID, and LPIPS metrics of all models. Our TAC-GAN again outperforms AC-GAN by a large margin. Compared to Projection cGAN, TAC-GAN is only slightly better when measured with LPIPS. In addition, TAC-GAN has lower IS than Projection cGAN. We hypothesize that TAC-GAN has a chance to generate images that do not belong to the given class in the overlap regions, because it aims to model the true conditional distribution.

4.5 VGGFace2

VGGFace2 [28] is a large-scale face recognition dataset, with around 362 images for each person. Its main difference to CIFAR100 and ImageNet1000 is that this dataset is more fine-grained with smaller intra-class diversities, making the generative task more difficult. We resize the center-cropped images to 64×64 . To compare different algorithms, we randomly choose 200 and 500 identities to construct the VGGFace200 and VGGFace500 datasets, respectively.

Figure 7 shows the generated face images for five randomly selected identities. AC-GAN collapses to the class center, generating very similar images for each class. Though Projection cGAN generate diverse images, it has blurry effects. Our TAC-GAN generates diverse and sharp images. To quantitatively compare the methods, we train a ResNet34 [41] classifier on the face data to calculate FID score. We report FID and LPIPS scores for all the methods in Table 1. It shows that TAC-GAN produces much better/lower FID score and slightly lower LPIPS score than Projection cGAN, which is consistent with the qualitative observations. These results suggest that TAC-GAN is a promising method for fine-grained datasets. More generated identities are attached in in section S9 of the SM.

5 Conclusion

In this paper, we have theoretically analyzed the low intra-class diversity problem of the widely used AC-GAN method from a distribution matching perspective. We showed that the auxiliary classifier in AC-GAN imposes perfect separability, which is disadvantageous when the supports of the class distributions have significant overlaps. Based on the analysis, we further proposed the Twin

Auxiliary Classifiers GAN (TAC-GAN) method, which introduces an additional auxiliary classifier to adversarially play with the players in AC-GAN. We demonstrated the efficacy of the proposed method both theoretically and empirically. TAC-GAN can resolve the issue of AC-GAN to learn an unbiased distribution, and generate high-quality samples on fine-grained image datasets.

References

- [1] I. Goodfellow, J. Pouget-Abadie, M. Mirza, B. Xu, D. Warde-Farley, S. Ozair, A. Courville, and Y. Bengio. Generative adversarial nets. In *NIPS*, 2014.
- [2] Sebastian Nowozin, Botond Cseke, and Ryota Tomioka. f-GAN: Training generative neural samplers using variational divergence minimization. In *NIPS*, pages 271–279, 2016.
- [3] Chun-Liang Li, Wei-Cheng Chang, Yu Cheng, Yiming Yang, and Barnabás Póczos. MMD GAN: Towards deeper understanding of moment matching network. In *NIPS*, pages 2203–2213, 2017.
- [4] Mikolaj Binkowski, Dougal J. Sutherland, Michael Arbel, and Arthur Gretton. Demystifying MMD GANs. *CoRR*, abs/1801.01401, 2018.
- [5] Alec Radford, Luke Metz, and Soumith Chintala. Unsupervised representation learning with deep convolutional generative adversarial networks. In *ICLR*, 2016.
- [6] Han Zhang, Ian J. Goodfellow, Dimitris N. Metaxas, and Augustus Odena. Self-attention generative adversarial networks. *arXiv:1805.08318*, 2018.
- [7] Tim Salimans, Ian Goodfellow, Wojciech Zaremba, Vicki Cheung, Alec Radford, and Xi Chen. Improved techniques for training GAN. In *NIPS*, pages 2234–2242, 2016.
- [8] Martin Arjovsky, Soumith Chintala, and Léon Bottou. Wasserstein generative adversarial networks. In *ICML*, pages 214–223, 2017.
- [9] Xudong Mao, Qing Li, Haoran Xie, Raymond YK Lau, Zhen Wang, and Stephen Paul Smolley. Least squares generative adversarial networks. In *ICCV*, pages 2794–2802, 2017.
- [10] Ishaan Gulrajani, Faruk Ahmed, Martin Arjovsky, Vincent Dumoulin, and Aaron C Courville. Improved training of wasserstein GAN. In *NIPS*, pages 5767–5777, 2017.
- [11] Lars Mescheder, Sebastian Nowozin, and Andreas Geiger. Which training methods for GANs do actually converge? In *ICML*, 2018.
- [12] Takeru Miyato, Toshiki Kataoka, Masanori Koyama, and Yuichi Yoshida. Spectral normalization for generative adversarial networks. In *ICLR*, 2018.
- [13] Andrew Brock, Jeff Donahue, and Karen Simonyan. Large scale GAN training for high fidelity natural image synthesis. In *ICLR*, 2019.
- [14] M. Mirza and S. Osindero. Conditional generative adversarial nets. *arXiv preprint arXiv:1411.1784*, 2014.
- [15] Phillip Isola, Jun-Yan Zhu, Tinghui Zhou, and Alexei A Efros. Image-to-image translation with conditional adversarial networks. *arxiv*, 2016.
- [16] Anh Nguyen, Jeff Clune, Yoshua Bengio, Alexey Dosovitskiy, and Jason Yosinski. Plug & play generative networks: Conditional iterative generation of images in latent space. In *CVPR*, pages 4467–4477, 2017.
- [17] Augustus Odena, Christopher Olah, and Jonathon Shlens. Conditional image synthesis with auxiliary classifier GANs. In *ICML*, pages 2642–2651. JMLR. org, 2017.
- [18] Dingdong Yang, Seunghoon Hong, Yunseok Jang, Tianchen Zhao, and Honglak Lee. Diversity-sensitive conditional generative adversarial networks. In *ICLR*, 2019.

[19] Scott Reed, Zeynep Akata, Xinchen Yan, Lajanugen Logeswaran, Bernt Schiele, and Honglak Lee. Generative adversarial text to image synthesis. In Maria Florina Balcan and Kilian Q. Weinberger, editors, *ICML*, pages 1060–1069, 2016.

[20] Han Zhang, Tao Xu, Hongsheng Li, Shaoting Zhang, Xiaogang Wang, Xiaolei Huang, and Dimitris N Metaxas. StackGAN: Text to photo-realistic image synthesis with stacked generative adversarial networks. In *ICCV*, pages 5907–5915, 2017.

[21] Emily L Denton, Soumith Chintala, Rob Fergus, et al. Deep generative image models using a laplacian pyramid of adversarial networks. In *NIPS*, pages 1486–1494, 2015.

[22] Guim Perarnau, Joost Van De Weijer, Bogdan Raducanu, and Jose M Álvarez. Invertible conditional gans for image editing. *arXiv preprint arXiv:1611.06355*, 2016.

[23] Vincent Dumoulin, Ishmael Belghazi, Ben Poole, Olivier Mastropietro, Alex Lamb, Martin Arjovsky, and Aaron Courville. Adversarially learned inference. *arXiv preprint arXiv:1606.00704*, 2016.

[24] Takeru Miyato and Masanori Koyama. cGANs with projection discriminator. In *ICLR*, 2018.

[25] Olga Russakovsky, Jia Deng, Hao Su, Jonathan Krause, Sanjeev Satheesh, Sean Ma, Zhiheng Huang, Andrej Karpathy, Aditya Khosla, Michael Bernstein, Alexander C. Berg, and Li Fei-Fei. ImageNet Large Scale Visual Recognition Challenge. *IJCV*, 115(3):211–252, 2015.

[26] Ayushman Dash, John Cristian Borges Gamboa, Sheraz Ahmed, Marcus Liwicki, and Muhammad Zeshan Afzal. Tac-gan-text conditioned auxiliary classifier generative adversarial network. *arXiv preprint arXiv:1703.06412*, 2017.

[27] Alex Krizhevsky, Vinod Nair, and Geoffrey Hinton. CIFAR-100 (canadian institute for advanced research).

[28] Qiong Cao, Li Shen, Weidi Xie, Omkar M. Parkhi, and Andrew Zisserman. Vggface2: A dataset for recognising faces across pose and age. In *FG*. IEEE Computer Society, 2018.

[29] Kumar Sricharan, Dennis Wei, and Alfred O Hero. Ensemble estimators for multivariate entropy estimation. *IEEE transactions on information theory*, 59(7):4374–4388, 2013.

[30] Shashank Singh and Barnabás Póczos. Finite-sample analysis of fixed-k nearest neighbor density functional estimators. In *NIPS*, pages 1217–1225, 2016.

[31] Weihao Gao, Sreeram Kannan, Sewoong Oh, and Pramod Viswanath. Estimating mutual information for discrete-continuous mixtures. In *NIPS*, pages 5986–5997, 2017.

[32] Chunyuan Li, Hao Liu, Changyou Chen, Yuchen Pu, Liqun Chen, Ricardo Henao, and Lawrence Carin. ALICE: Towards understanding adversarial learning for joint distribution matching. In *NIPS*, 2017.

[33] Rui Shu, Hung Bui, and Stefano Ermon. Ac-gan learns a biased distribution.

[34] Yann LeCun. The MNIST database of handwritten digits. <http://yann.lecun.com/exdb/mnist/>.

[35] Emanuel Parzen. On estimation of a probability density function and mode. *The annals of mathematical statistics*, 1962.

[36] Arthur Gretton, Karsten M. Borgwardt, Malte J. Rasch, Bernhard Schölkopf, and Alexander Smola. A kernel two-sample test. *J. Mach. Learn. Res.*, 2012.

[37] Yanping Huang, Yonglong Cheng, Dehao Chen, HyoukJoong Lee, Jiquan Ngiam, Quoc V Le, and Zhifeng Chen. Gpipe: Efficient training of giant neural networks using pipeline parallelism. *arXiv preprint arXiv:1811.06965*, 2018.

[38] Tim Salimans, Ian J. Goodfellow, Wojciech Zaremba, Vicki Cheung, Alec Radford, and Xi Chen. Improved techniques for training gans. *CoRR*, abs/1606.03498, 2016.

- [39] Martin Heusel, Hubert Ramsauer, Thomas Unterthiner, Bernhard Nessler, Günter Klambauer, and Sepp Hochreiter. Gans trained by a two time-scale update rule converge to a nash equilibrium. *CoRR*, abs/1706.08500, 2017.
- [40] Richard Zhang, Phillip Isola, Alexei A Efros, Eli Shechtman, and Oliver Wang. The unreasonable effectiveness of deep features as a perceptual metric. In *CVPR*, pages 586–595, 2018.
- [41] Kaiming He, Xiangyu Zhang, Shaoqing Ren, and Jian Sun. Deep residual learning for image recognition. In *CVPR*, pages 770–778, 2016.

Supplementary Materials for “Twin Auxiliary Classifiers GAN”

This supplementary material provides the proofs and more experimental details which are omitted in the submitted paper. The equation numbers in this material are consistent with those in the paper.

S1. Proof of Theorem 1

Proof. The optimal $Q_{Y|X}^*$ is obtained by the following optimization problem:

$$\begin{aligned} \min_{Q_{Y|X}} - \mathbb{E}_{(X,Y) \sim Q_{XY}} [\log Q^c(Y|X)] &= - \mathbb{E}_{X \sim Q_X} [\sum_{i=1}^K Q(Y = i|X) \log Q^c(Y = i|X)], \\ \text{s.t. } \sum_{i=1}^K Q(Y = i|X = x) &= 1 \text{ and } Q(Y = i|X = x) \geq 0. \end{aligned} \quad (\text{E1})$$

The optimization problem in (E1) is equivalent to minimizing the objective point-wisely for each x , i.e.,

$$\begin{aligned} \min_{Q_{Y|X=x}} - \sum_{i=1}^K Q(Y = i|X = x) \log Q^c(Y = i|X = x), \\ \text{s.t. } \sum_{i=1}^K Q(Y = i|X = x) &= 1 \text{ and } Q(Y = i|X = x) \geq 0, \end{aligned} \quad (\text{E2})$$

which is a linear programming (LP) problem. The optimal solution must lie in the extreme points of the feasible set, which are those points with posterior probability 1 for one class and 0 for the other classes. By evaluating the objective values of these extreme points, the optimal solution is (5) with objective value $-\log Q^c(Y = k|X = x)$, where $k = \arg \max_i Q^c(Y = i|X = x)$. \square

S2. Proof of Theorem 2

Proof. The minimax game (7) can be written as

$$\begin{aligned} \min_G \max_{C^{mi}} V(G, C^{mi}) &= \mathbb{E}_{Z \sim P_Z, Y \sim P_Y} [\log(C^{mi}(G(Z, Y), Y))] \\ &= \mathbb{E}_{X \sim Q_{XY}} [\log(C^{mi}(X, Y))] \\ &= \frac{1}{K} \sum_{k=1}^K \mathbb{E}_{X \sim Q_{X|Y=k}} [\log(C^{mi}(X, Y = k))] \\ \text{s.t. } \sum_{k=1}^K C^{mi}(X, Y = k) &= 1, \end{aligned} \quad (\text{E3})$$

where the constraint is because C^{mi} is forced to have probability outputs that sum to one. In the following proposition, we will give the optimal C^{mi} for any given G , or equivalently Q_{XY} .

Proposition 1. *Let for a fixed generator G , the optimal prediction probabilities $C^{mi}(X = x, Y = k)$ of C^{mi} are*

$$C^{mi*}(x, Y = k) = \frac{Q(x|Y = k)}{\sum_{k'=1}^K Q(x|Y = k')}. \quad (\text{E4})$$

Proof. For a fixed G , (E3) reduces to maximize the value function $V(G, C^{mi})$ w.r.t. $C^{mi}(x, Y = 1), \dots, C^{mi}(x, Y = K)$:

$$\begin{aligned} & \{C^{mi*}(x, Y = 1), \dots, C^{mi*}(x, Y = K)\} \\ &= \arg \max_{C^{mi}(x, Y=1), \dots, C^{mi}(x, Y=K)} \sum_{k=1}^K \int_x Q(x|Y=k) \log(C^{mi}(x, Y=k)) dx \\ & \quad s.t. \sum_{k=1}^K C^{mi}(x, Y=k) = 1. \end{aligned} \quad (\text{E5})$$

By maximizing the value function pointwisely and applying Lagrange multipliers, we obtain the following problem:

$$\begin{aligned} & \{C^{mi*}(x, Y = 1), \dots, C^{mi*}(x, Y = K)\} \\ &= \arg \max_{C^{mi}(x, Y=1), \dots, C^{mi}(x, Y=K)} \sum_{k=1}^K Q(x|Y=k) \log(C^{mi}(x, Y=k)) \\ & \quad + \lambda \left(\sum_{k=1}^K C^{mi}(x, Y=k) - 1 \right). \end{aligned} \quad (\text{E6})$$

Setting the derivative of (E6) w.r.t. $C^{mi}(x, Y = k)$ to zeros, we obtain

$$C^{mi*}(x, Y = k) = -\frac{Q(x|Y=k)}{\lambda}. \quad (\text{E7})$$

We can solve for the Lagrange multiplier λ by substituting (E7) into the constraint $\sum_{k=1}^K C^{mi}(x, Y = k) = 1$ to give $\lambda = -\sum_{k=1}^K Q(x|Y=k)$. Thus we obtain the optimal solution

$$C^{mi*}(x, Y = k) = \frac{Q(x|Y=k)}{\sum_{k'=1}^K Q(x|Y=k')}. \quad (\text{E8})$$

□

Now we are ready to prove the theorem. If we add $K \log K$ to $U(G)$, we can obtain:

$$\begin{aligned} & U(G) + K \log K \\ &= \sum_{k=1}^K \mathbb{E}_{X \sim Q(X|Y=k)} \left[\log \frac{Q(X|Y=k)}{\sum_{k'=1}^K Q(X|Y=k')} \right] + K \log K \\ &= \sum_{k=1}^K \mathbb{E}_{X \sim Q(X|Y=k)} \left[\log \frac{Q(X|Y=k)}{\frac{1}{K} \sum_{k'=1}^K Q(X|Y=k')} \right] \\ &= \sum_{m=1}^K KL \left(Q(X|Y=k) \middle\| \frac{1}{K} \sum_{k=1}^K Q(X|Y=k') \right). \end{aligned} \quad (\text{E9})$$

By using the definition of JSD, we have

$$U(G) = -K \log K + K \cdot \text{JSD}(Q_{X|Y=1}, \dots, Q_{X|Y=K}). \quad (\text{E10})$$

Since the Jensen-Shannon divergence among multiple distributions is always non-negative, and zero if they are equal, we have shown that $U^* = -K \log K$ is the global minimum of $U(G)$ and that the only solution is $Q_{X|Y=1} = Q_{X|Y=2} = \dots = Q_{X|Y=K}$. □

S3. Proof of Theorem 3

According to the triangle inequality of total variation (TV) distance, we have

$$d_{TV}(P_{XY}, Q_{XY}) \leq d_{TV}(P_{XY}, P_{Y|X}Q_X) + d_{TV}(P_{Y|X}Q_X, Q_{XY}). \quad (\text{E11})$$

Using the definition of TV distance, we have

$$\begin{aligned}
d_{TV}(P_{Y|X}P_X, P_{Y|X}Q_X) &= \frac{1}{2} \int |P_{Y|X}(y|x)P_X(x) - P_{Y|X}(y|x)Q_X(x)|\mu(x, y) \\
&\stackrel{(a)}{\leq} \frac{1}{2} \int |P_{Y|X}(y|x)|\mu(x, y) \int |P_X(x) - Q_X(x)|\mu(x) \\
&\leq c_1 d_{TV}(P_X, Q_X),
\end{aligned} \tag{E12}$$

where P and Q are densities, μ is a (σ -finite) measure, c_1 is an upper bound of $\frac{1}{2} \int |P_{Y|X}(y|x)|\mu(x, y)$, and (a) follows from the Hölder inequality.

Similarly, we have

$$d_{TV}(P_{Y|X}Q_X, Q_{Y|X}Q_X) \leq c_2 d_{TV}(P_{Y|X}, Q_{Y|X}), \tag{E13}$$

where c_2 is an upper bound of $\frac{1}{2} \int |Q_X(x)|\mu(x)$. Combining (E11), (E12), and (E13), we have

$$\begin{aligned}
d_{TV}(P_{XY}, Q_{XY}) &\leq c_1 d_{TV}(P_X, Q_X) + c_2 d_{TV}(P_{Y|X}, Q_{Y|X}) \\
&\leq c_1 d_{TV}(P_X, Q_X) + c_2 d_{TV}(P_{Y|X}, Q_{Y|X}^c) + c_2 d_{TV}(Q_{Y|X}, Q_{Y|X}^c).
\end{aligned} \tag{E14}$$

According to the Pinsker inequality $d_{TV}(P, Q) \leq \sqrt{\frac{KL(P||Q)}{2}}$ [1], and the relation between TV and JSD, *i.e.*, $\frac{1}{2}d_{TV}(P, Q)^2 \leq JSD(P, Q) \leq 2d_{TV}(P, Q)$ [2], we can rewrite (E14) as

$$JSD(P_{XY}, Q_{XY}) \leq 2c_1 \sqrt{2JSD(P_X, Q_X)} + c_2 \sqrt{2KL(P_{Y|X}||Q_{Y|X}^c)} + c_2 \sqrt{2KL(Q_{Y|X}||Q_{Y|X}^c)}. \tag{E15}$$

S4. 1D MoG synthetic Data

S4.1. Experimental Setup

For all the networks in AC-GAN, Projection cGAN, and our TAC-GAN, we adopt the three layer Multi-Layer Perceptron (MLP) with hidden dimension 10 and Relu [3] activation function. The only difference is the number of input and output nodes. We choose Adam [4] as the optimizer and set the learning rate as 2e-4 and the hyperparameter of Adam as $\beta = (0.0, 0.999)$. We train 10 steps for D , C , and C^{mi} and 1 step for G in every iteration. The batch size is set to 256.

S4.2. More Results

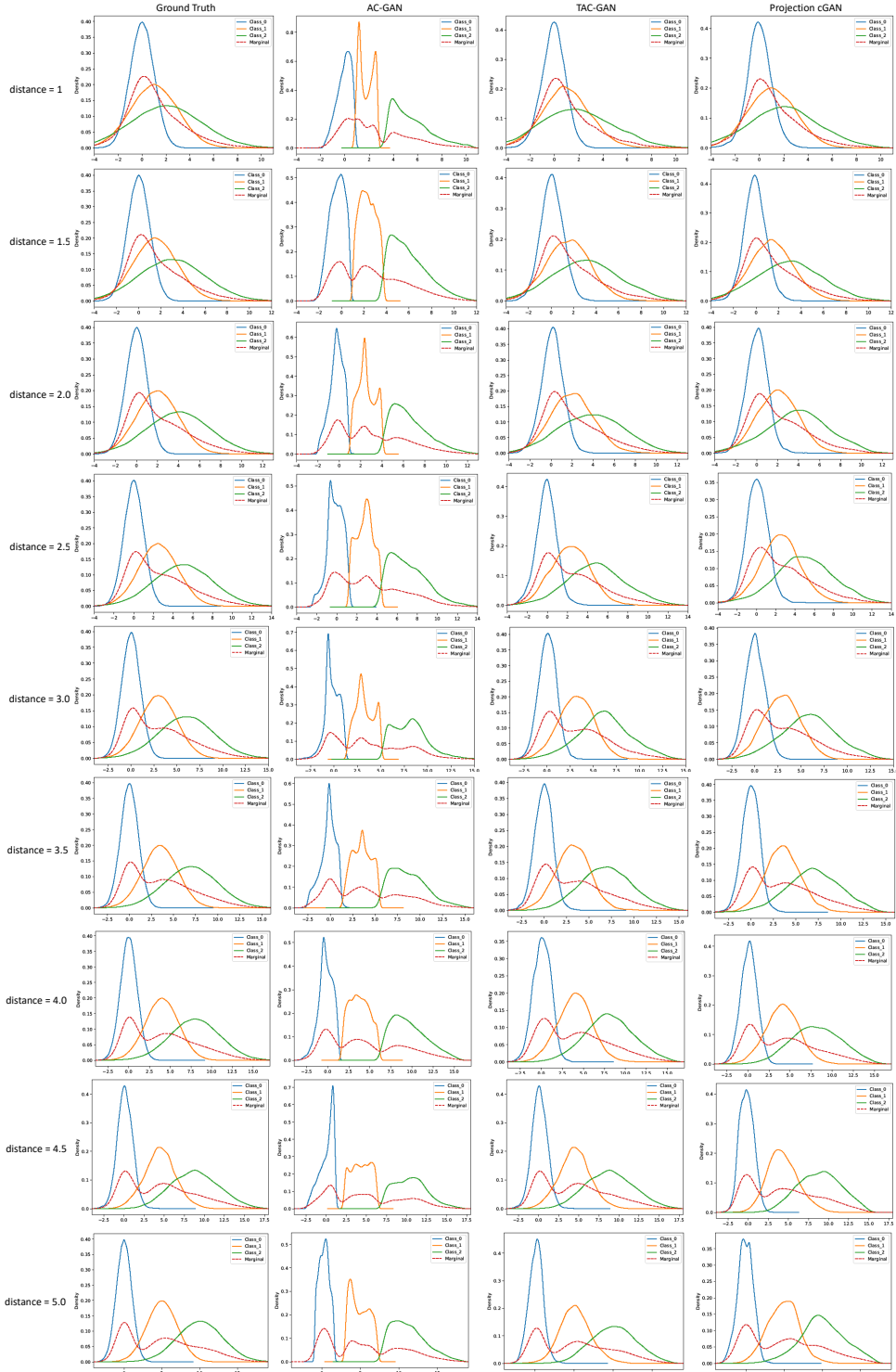


Figure 8: Change distance between the means of adjacent 1-D Gaussian Components, in this figure, all models adopt cross entropy loss.

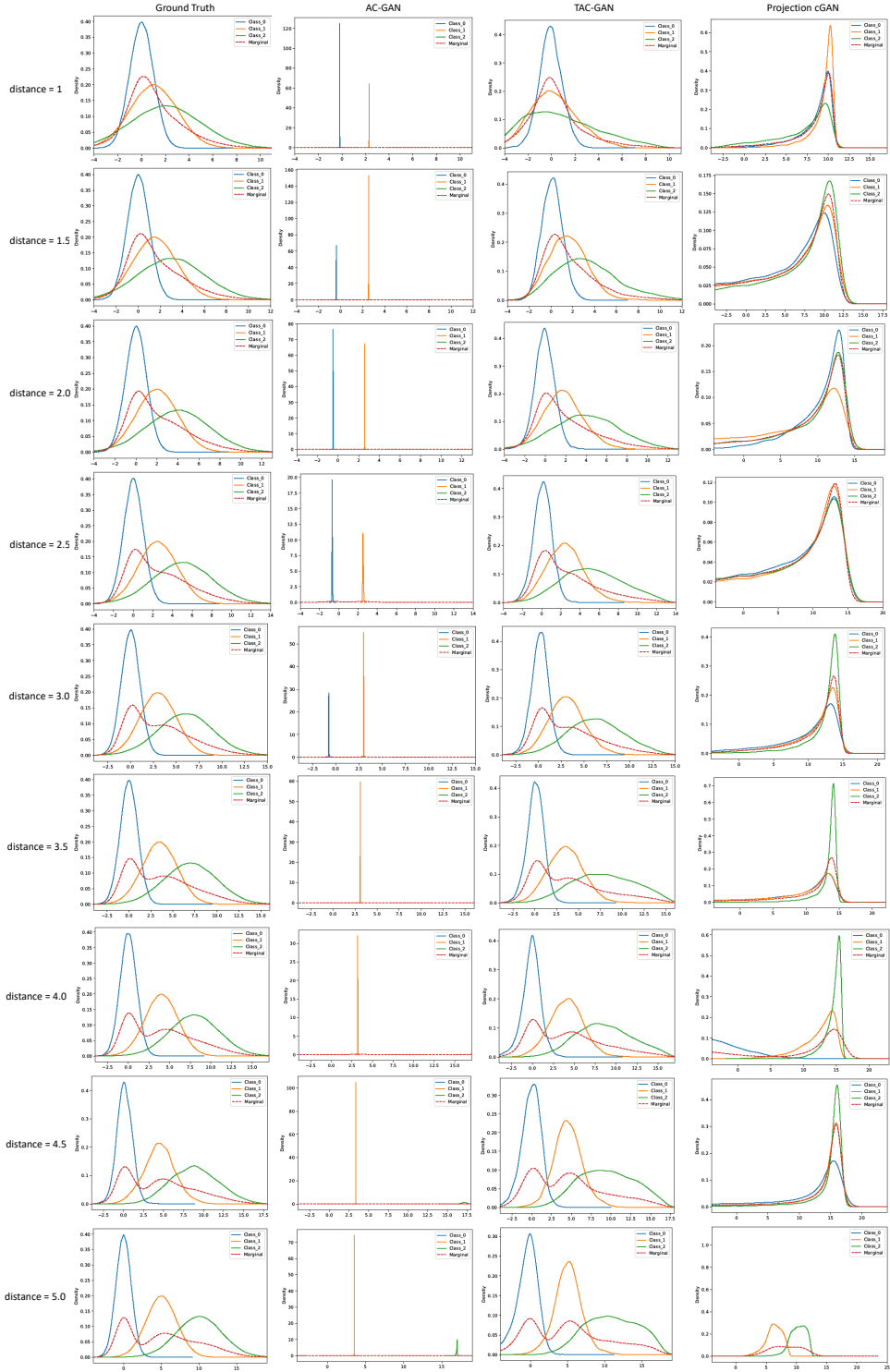


Figure 9: Change distance between the means of adjacent 1-D Gaussian Components, in this figure, all models adopt hinge loss.

S5. 2D MoG Synthetic Data

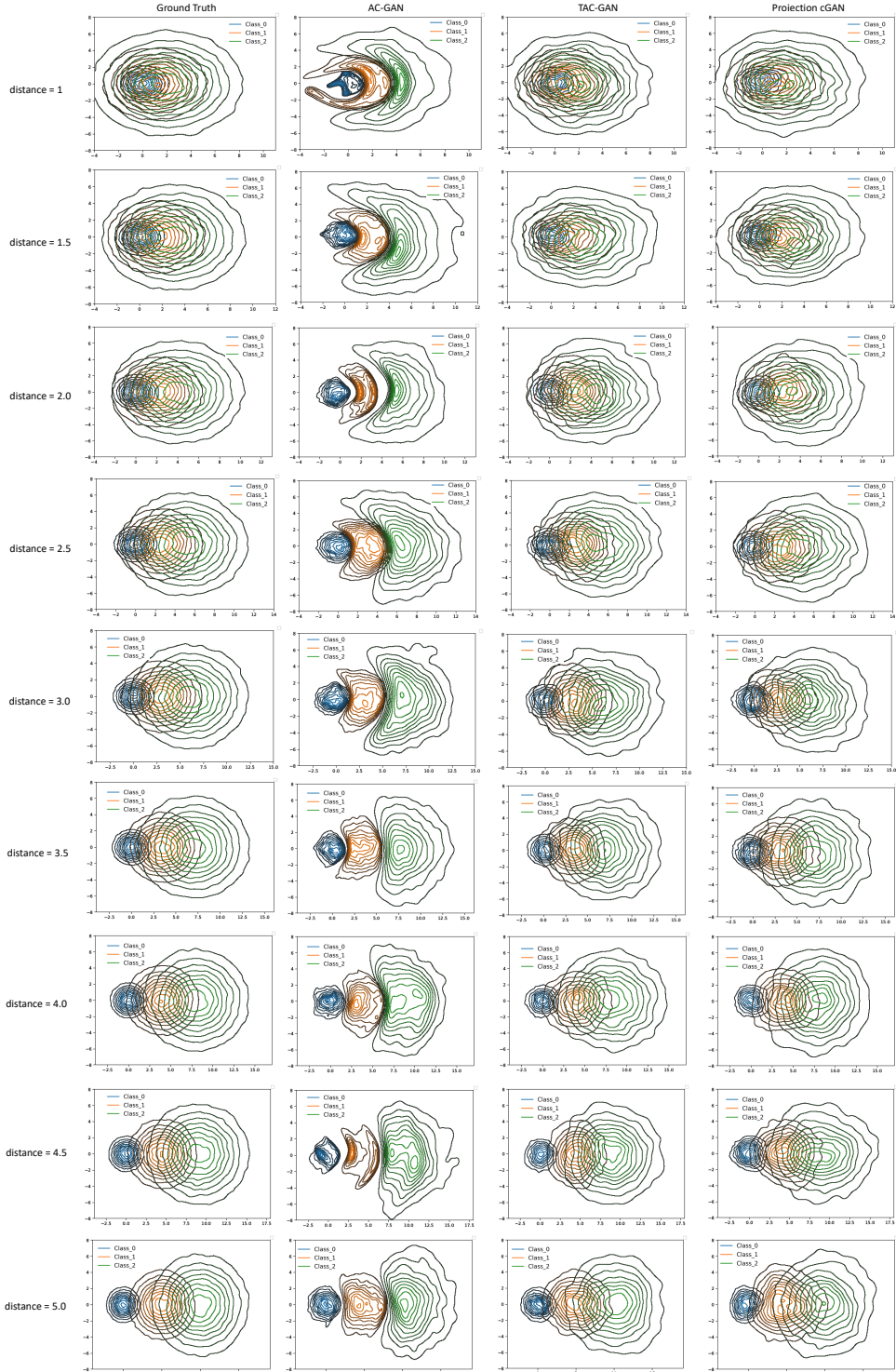


Figure 10: Change distance between the means of adjacent 2-D Gaussian Components in x-axis, in this figure, all models adopt cross entropy loss.

S6. Overlapping MNIST

S6.1. Experimental Setup

For the network settings, the G network consists of three layers of Res-Block and relies on Conditional Batch Normalization (CBN) [5] to plug in label information. The network structure of D mirrors G network without CBN. To stabilize training, D, C, C^{mi} share the the convolutional layers and differ in the fully-connected layers. The chosen dimension of latent z is 128 and optimizer is Adam with learning rate $lr=2e-4$ and $\beta = \{0.0, 0.999\}$ for both G and D networks. Each iteration contains 2 steps of D, C, C^{mi} training and 1 step of G training. The batch size is set to 100.

S6.2. More Results

In this experiment, we fix the training data and change the weight of classifier from $\lambda_c = 0.5$ to $\lambda_c = 3.0$ with step 0.5 for our model TAC-GAN and AC-GAN. For AC-GAN, when the value of λ_c becomes larger, the proportion of the generated digit ‘0’, which is the overlapping digit, goes smaller. However, our model is still able to replicate the true distribution.

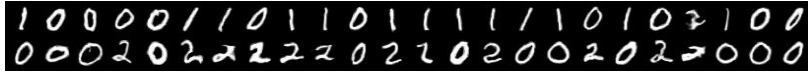
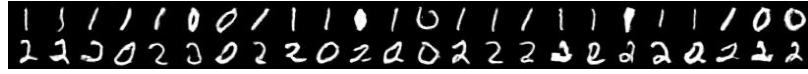
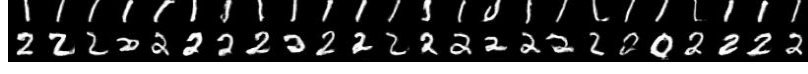
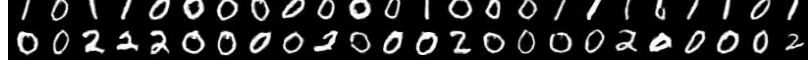
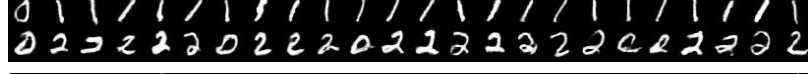
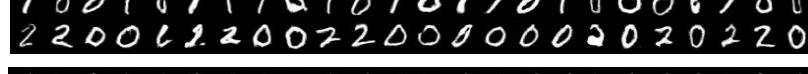
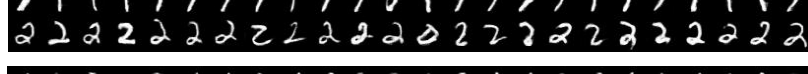
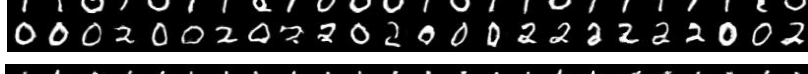
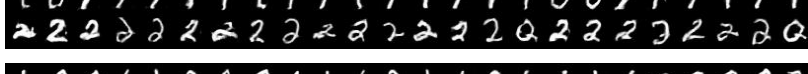
Real Data	
AC-GAN, $\lambda_c = 0.5$	
TAC-GAN, $\lambda_c = 0.5$	
AC-GAN, $\lambda_c = 1.0$	
TAC-GAN, $\lambda_c = 1.0$	
AC-GAN, $\lambda_c = 1.5$	
TAC-GAN, $\lambda_c = 1.5$	
AC-GAN, $\lambda_c = 2.0$	
TAC-GAN, $\lambda_c = 2.0$	
AC-GAN, $\lambda_c = 2.5$	
TAC-GAN, $\lambda_c = 2.5$	
AC-GAN, $\lambda_c = 3.0$	
TAC-GAN, $\lambda_c = 3.0$	

Figure 11: More generated results for the overlapping MNIST dataset.

S7. CIFAR100

S7.1. Experimental Setup

Due to the complexity and diversity of this dataset, we apply the latest SN-GAN [6] as our base model, the implementation is based on Pytorch implementation of Big-GAN [7] and SN layer is added to both G and D networks [8]. On this dataset, there is no need to add Self-Attention layer [8] and only three Res-Blocks layers are applied due to the low resolution as 32×32 . As done by SN-GAN [6], we replace the loss term ④ by the hinge loss in order to stabilize the GAN training part. For all evaluated methods, the batch size is 100 and total number of training iterations is 60K. The optimizer parameters are identical to those used in the overlapping MNIST experiment.

S7.2. More Results

We show the generated samples for all classes in Figure 12 and report the FID and LPIPS scores for each class in Figure 13 and Figure 14, respectively.



Figure 12: 100 classes of CIFAR100 generated samples, we choose the classifier weight $\lambda_c = 0.2$ for AC-GAN model.

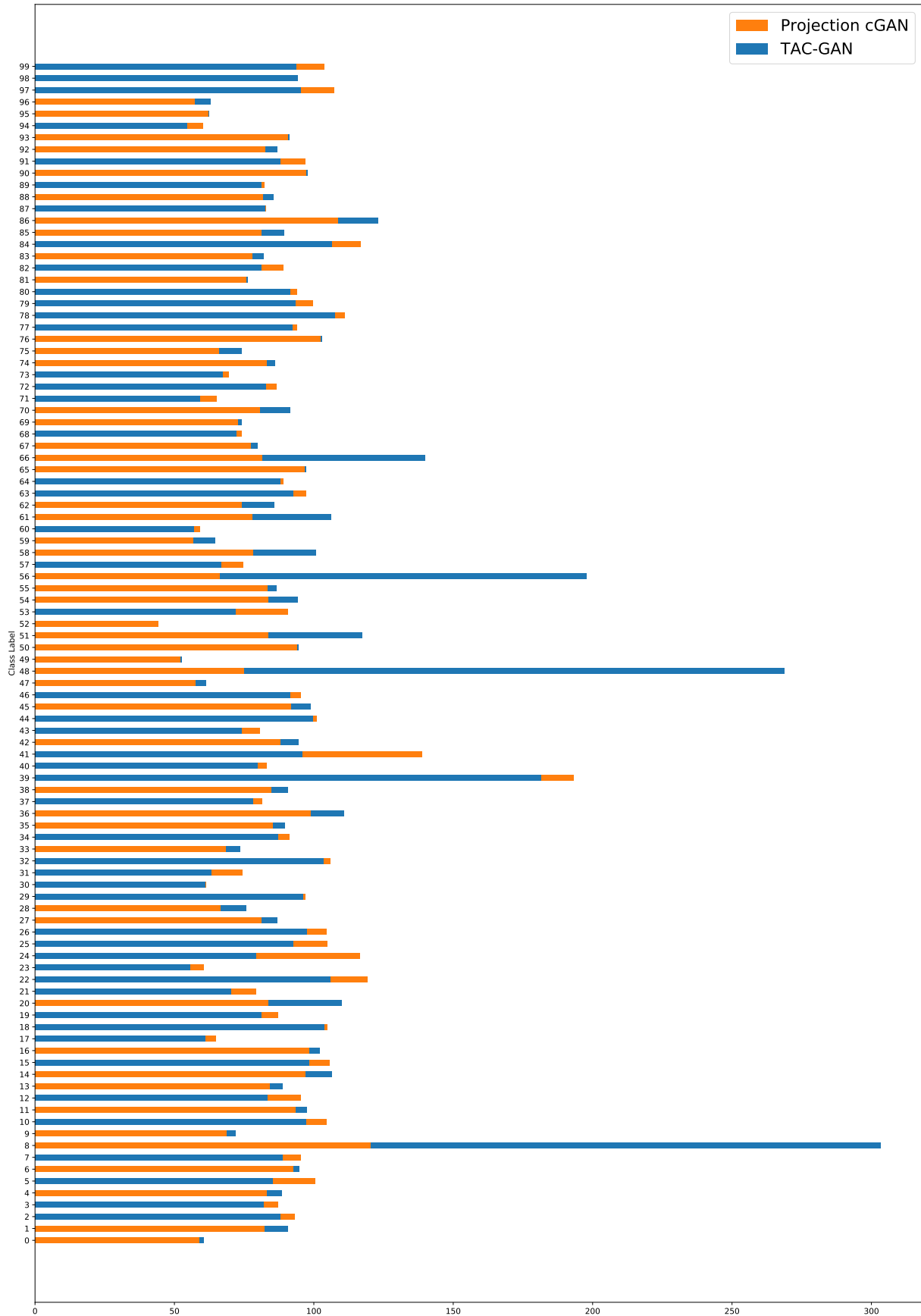


Figure 13: The FID score is reported for each class on CIFAR100 generated data, lower is better. The y axis denotes class label and x axis denotes FID score.

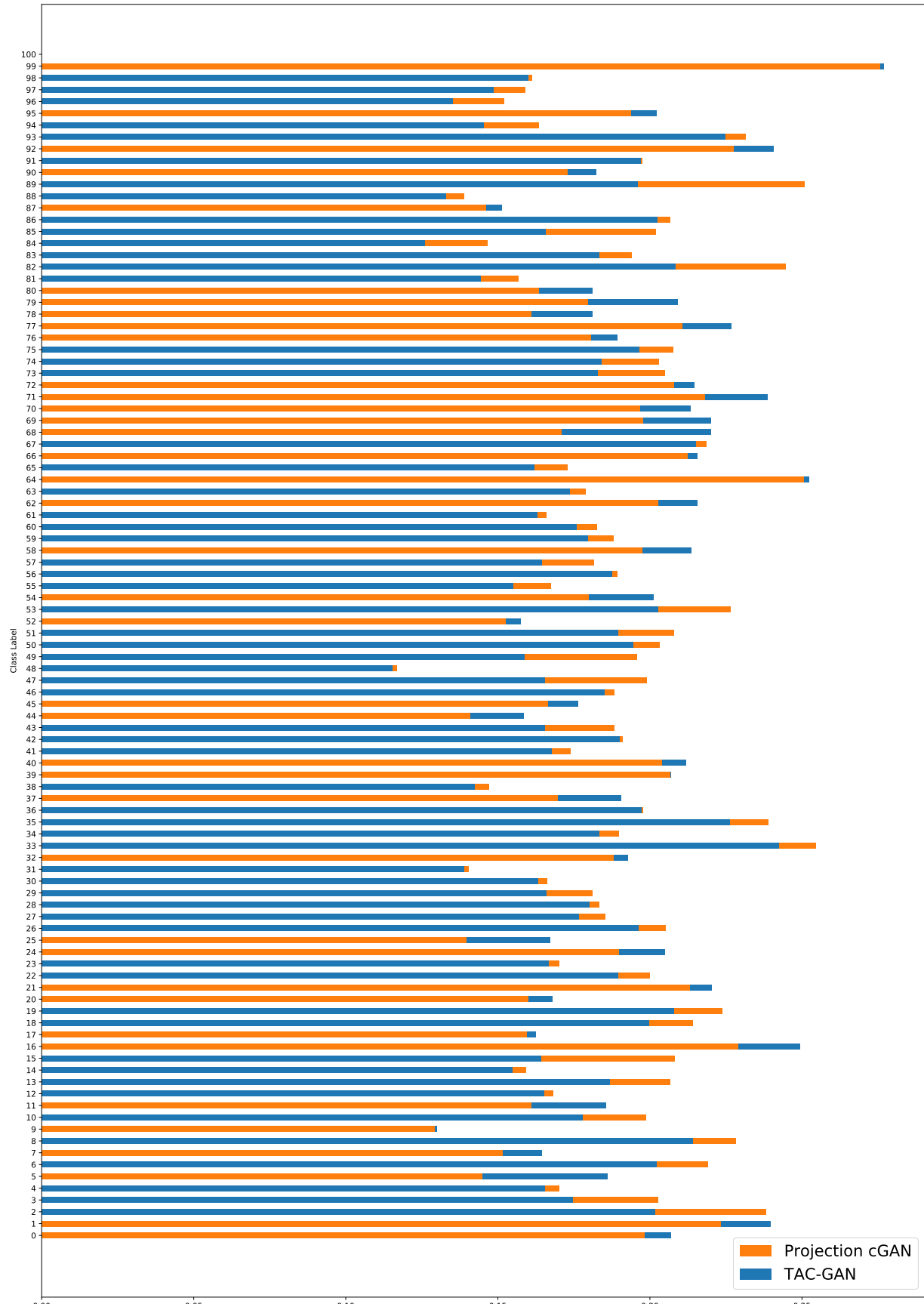


Figure 14: The LPIPS score is reported for each class on CIFAR100 generated data, larger values means better variance inner class. The y axis denotes class label and x axis denotes LPIPS score.

S8. ImageNet1000

S8.1. Experimental Setup

We adopt the full version of Big-GAN model architecture as the base network for AC-GAN, Projection cGAN, and TAC-GAN. In this experiment, we apply the shared class embedding for each CBN layer in G model, and feed noise z to multiple layers of G by concatenating with class embedding vector. We use orthogonal initialization for network parameters [7]. In addition, following [7], we add Self-Attention layer with the resolution of 64 for ImageNet. Due to limited computational resources, we fix the batch size to 256. To boost the training speed, we only train one step for D network and one step for G network.

S8.2. More Results



Figure 15: In this figure, we randomly select some generated samples from 1000 classes. It contains birds, snakes, bug, dog, food, scene, etc. Our model shows a very competitive fidelity and diversity. Generative models are all trained on ImageNet1000 and the image resolution is 128×128 .

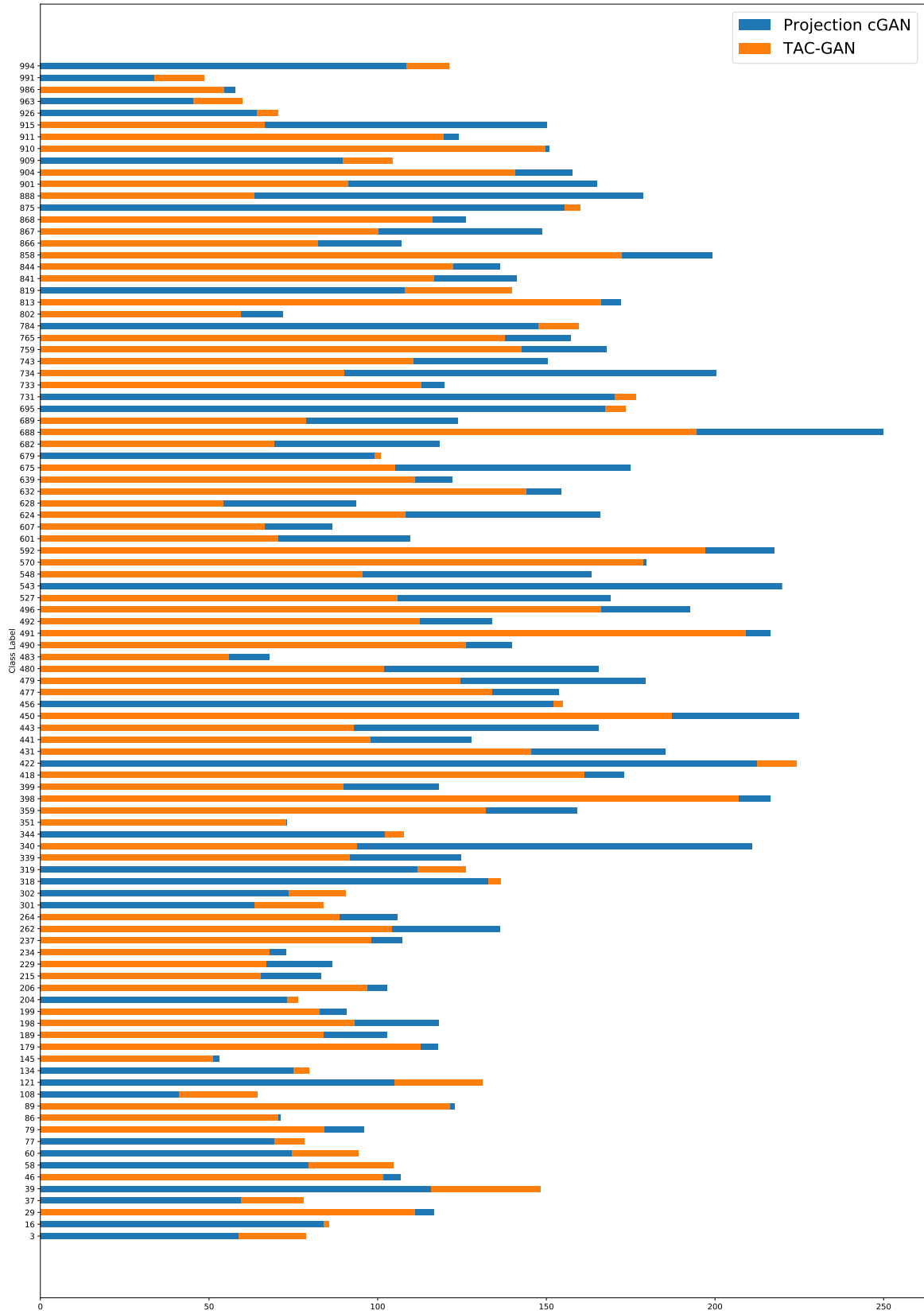


Figure 16: The FID score is reported for each class on ImageNet1000 generated data, we randomly select 100 classes from our generated samples for comparison between our model TAC-GAN and Projection cGAN. The method with a lower FID score is better. The y axis denotes class label and x axis denotes FID score.

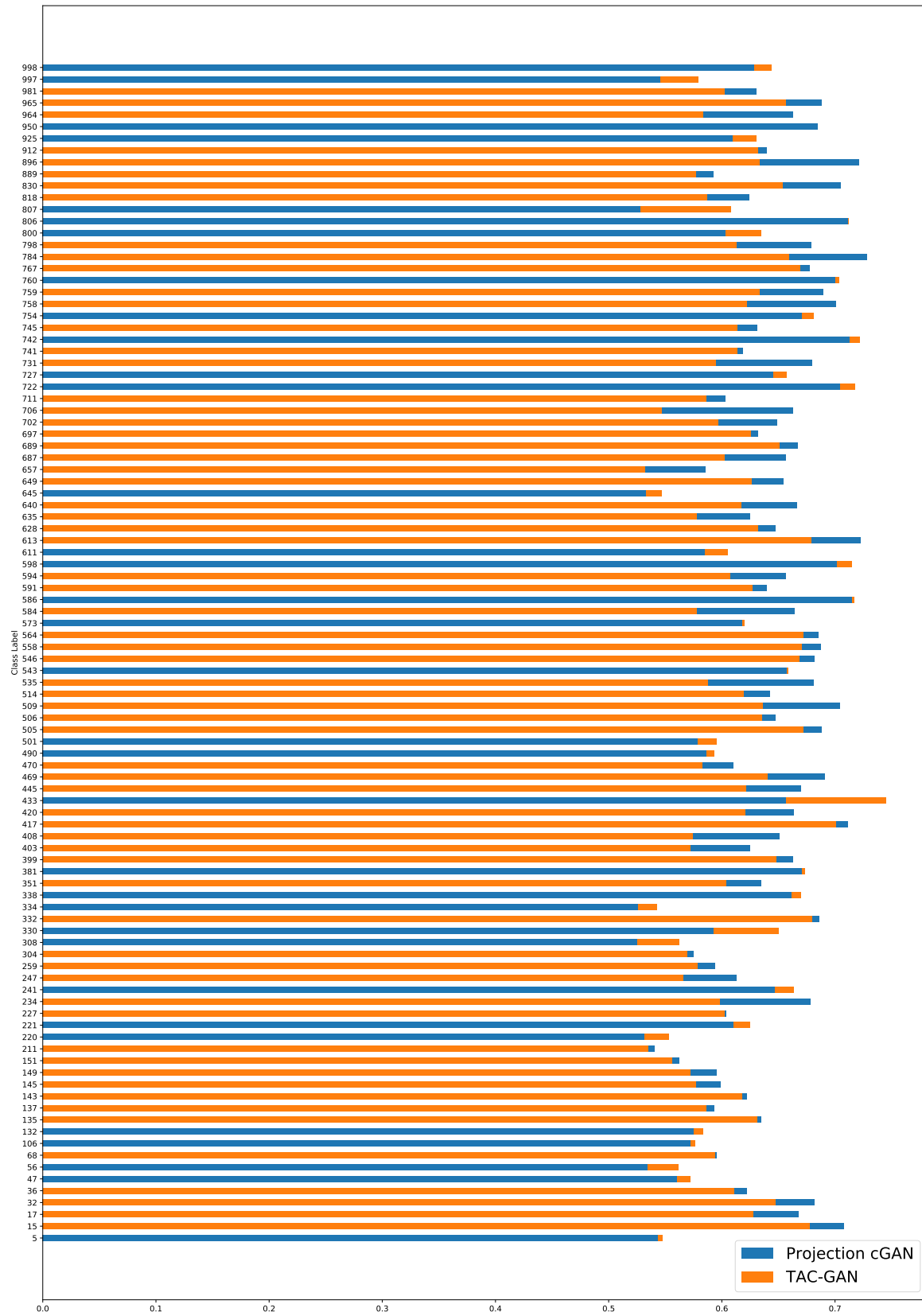


Figure 17: The LPIPS score is reported for each class on ImageNet1000 generated data. we randomly select 100 classes from our generated samples for comparison between our model TAC-GAN and Projection cGAN, higher LPIPS score means larger intra-class variance. The y axis denotes class label and x axis denotes LPIPS score.

S9. VGGFace200

S9.1. Experimental Setup

We adopt the full version of Big-GAN model architecture as the base network for AC-GAN, Projection cGAN, and TAC-GAN. In this experiment, we apply the shared class embedding for each CBN layer in G model, and feed noise z to multiple layers of G by concatenating with class embedding vector. We use orthogonal initialization for network parameters [7]. In addition, following [7], we add Self-Attention layer with the resolution of 32 for VGGFace. Due to limited computational resources, we fix the batch size to 256. In this setting, we train two steps for D network and two steps for G network. The only difference of the networks applied on ImageNet and VGGFace is that the network on ImageNet has one additional up-sampling block and one more down-sampling block added to G and D Networks to accommodate higher resolution.

S9.2. More Results



Figure 18: In this figure, we randomly select some generated samples for illustration. All the generative models are trained on 200 classes on the randomly sampled 200 classes from the VGGFace2 dataset.

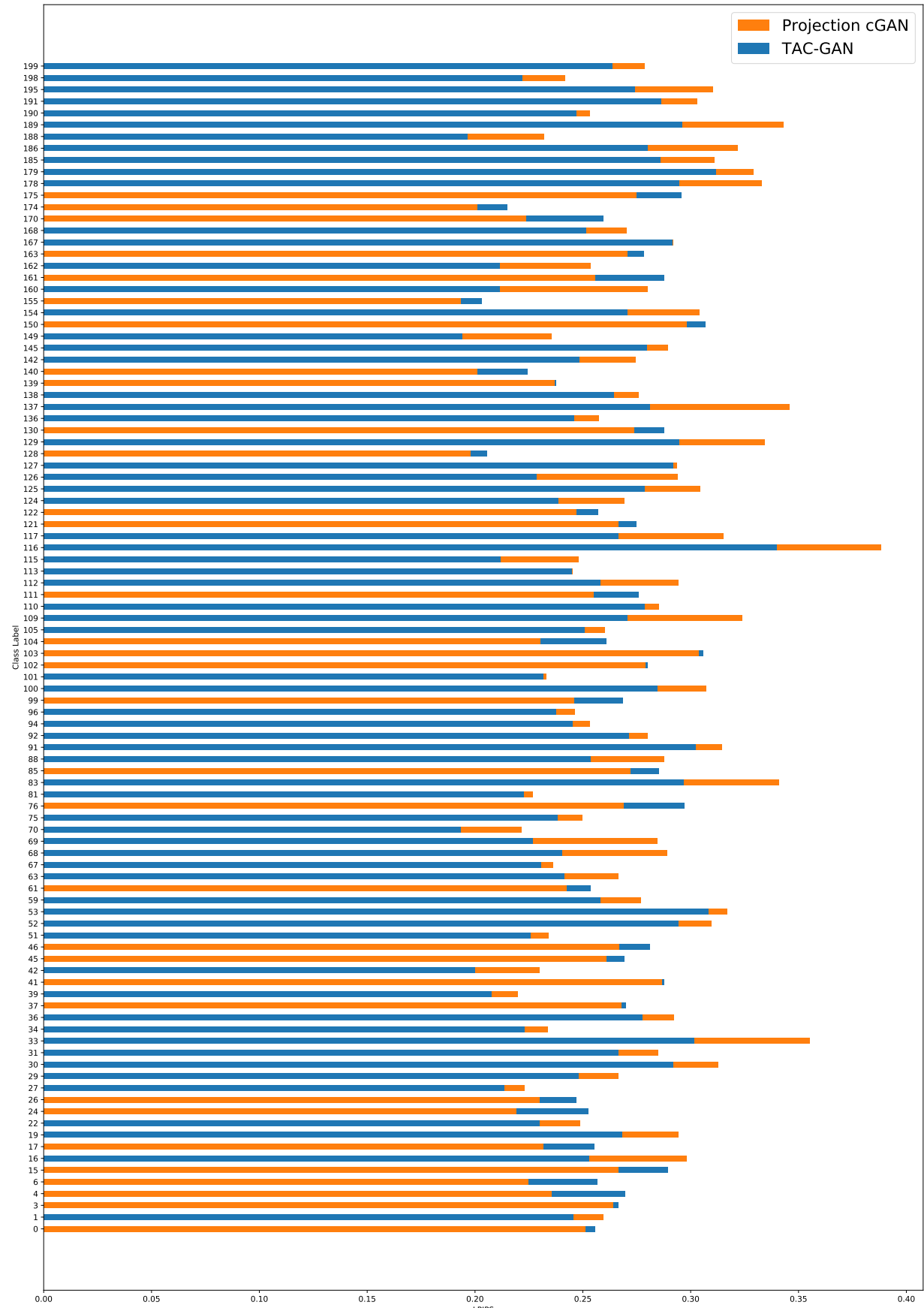


Figure 19: The LPIPS score is reported for each class on VGGFace200 generated data. we randomly select 100 classes from our generated samples for comparison between our model TAC-GAN and Projection cGAN, higher LPIPS score means larger intra-class variance. The y axis denotes class label and x axis denotes LPIPS score.

References

- [1] Alexandre B. Tsybakov. *Introduction to Nonparametric Estimation*. Springer Publishing Company, Incorporated, 1st edition, 2008.
- [2] Kiran K Thekumparampil, Ashish Khetan, Zinan Lin, and Sewoong Oh. Robustness of conditional gans to noisy labels. In *NeurIPS*, pages 10271–10282. Curran Associates, Inc., 2018.
- [3] Vinod Nair and Geoffrey E. Hinton. Rectified linear units improve restricted boltzmann machines. In *ICML*, 2010.
- [4] Diederik P. Kingma and Jimmy Ba. Adam: A method for stochastic optimization. *CoRR*, abs/1412.6980, 2015.
- [5] Harm de Vries, Florian Strub, Jérémie Mary, Hugo Larochelle, Olivier Pietquin, and Aaron C. Courville. Modulating early visual processing by language. *CoRR*, abs/1707.00683, 2017.
- [6] Takeru Miyato, Toshiki Kataoka, Masanori Koyama, and Yuichi Yoshida. Spectral normalization for generative adversarial networks. In *ICLR*, 2018.
- [7] Andrew Brock, Jeff Donahue, and Karen Simonyan. Large scale GAN training for high fidelity natural image synthesis. In *ICLR*, 2019.
- [8] Han Zhang, Ian J. Goodfellow, Dimitris N. Metaxas, and Augustus Odena. Self-attention generative adversarial networks. *arXiv:1805.08318*, 2018.